Mammalian SEPT9 isoforms direct microtubule-dependent arrangements of septin core heteromers

Mikael E. Sellin[a,b], Sonja Stenmark[a], and Martin Gullberg[a]
[a]Department of Molecular Biology, Umeå University, SE-901 87 Umeå, Sweden; [b]Institute of Microbiology, D-BIOL, ETH Zürich, 8093 Zürich, Switzerland

ABSTRACT Septin-family proteins assemble into rod-shaped heteromeric complexes that form higher-order arrangements at the cell cortex, where they serve apparently conserved functions as diffusion barriers and molecular scaffolds. There are 13 confirmed septin paralogues in mammals, which may be ubiquitous or tissue specific. Septin hetero-oligomerization appears homology subgroup directed, which in turn determines the subunit arrangement of six- to eight-subunit core heteromers. Here we address functional properties of human SEPT9, which, due to variable mRNA splicing, exists as multiple isoforms that differ between tissues. Myeloid K562 cells express three SEPT9 isoforms, all of which have an equal propensity to hetero-oligomerize with SEPT7-containing hexamers to generate octameric heteromers. However, due to limiting amounts of SEPT9, K562 cells contain both hexameric and octameric heteromers. To generate cell lines with controllable hexamer-to-octamer ratios and that express single SEPT9 isoforms, we developed a gene product replacement strategy. By this means we identified SEPT9 isoform–specific properties that either facilitate septin heteromer polymerization along microtubules or modulate the size range of submembranous septin disks—a prevalent septin structure in nonadhered cells. Our findings show that the SEPT9 expression level directs the hexamer-to-octamer ratio, and that the isoform composition and expression level together determine higher-order arrangements of septins.

INTRODUCTION

Members of the septin protein family have conserved functions for plasma membrane compartmentalization of animal and fungal cells. Septins polymerize into a variety of higher-order arrangements that may interact with phosphatidylinositol-4,5-bisphosphate–containing lipid bilayers, actin filaments, and/or microtubules (Kinoshita *et al.*, 2002; Surka *et al.*, 2002; Tanaka-Takiguchi *et al.*, 2009; Bertin *et al.*, 2010; Garrenton *et al.*, 2010; Bowen *et al.*, 2011; Sellin *et al.*, 2011a),

but the molecular details of these interactions are far from clear (reviewed in Oh and Bi, 2011). Mammals have 13 genes encoding both ubiquitous and tissue-specific septin paralogues (*SEPT1-12* and *SEPT14* in humans; the former *SEPT13* is a pseudogene), which have inferred roles in a wide variety of cellular functions (reviewed in Beise and Trimble, 2011). Cross-kingdom comparisons have not provided any indications concerning orthologous relationships between the multitude of septin paralogues present in animals and fungi (Cao *et al.*, 2007; Pan *et al.*, 2007). However, all metazoan septins can readily be classified into four subgroups, termed the SEPT2, SEPT3, SEPT6, and SEPT7 subgroups after their founding member (reviewed in Kinoshita, 2003). Each of these four subgroups appears to be represented in chordates but only two or three among invertebrates (Cao *et al.*, 2007).

Rod-shaped heteromeric septin complexes have been visualized by electron microscopy (Field *et al.*, 1996; John *et al.*, 2007; Sirajuddin *et al.*, 2007; Bertin *et al.*, 2008). These represent core heteromers and comprise from four to eight subunits, depending on the organism. At low ionic strength, these core heteromers

polymerize via end-to-end joining and lateral interactions (reviewed in Weirich et al., 2008; Mostowy and Cossart, 2012), a process that is facilitated by interactions with actin filaments and lipid bilayers (Kinoshita et al., 2002; Tanaka-Takiguchi et al., 2009; Bertin et al., 2010). Crystal structures of bacterially expressed human septins have identified two interaction interfaces—denoted the G- and NC-interfaces—on the conserved GTP-binding "G-domain" (Sirajuddin et al., 2007, 2009). It was shown that each septin subunit associates with its neighbors through either a G-interface or an NC-interface, which provides a universal principle by which septins assemble into core heteromers, as well as extended filaments.

In contrast to less complex fungal model systems, the assembly states and hetero-oligomerization partners of the 13 mammalian septin paralogues have been elusive (reviewed in Oh and Bi, 2011). We recently explored the native assembly states and subunit interchangeability within the human septin system. The data indicate that mammalian septins exist predominantly in the context of six to eight subunit heteromers that depend on SEPT7 for stability (Sellin et al., 2011b). The six subunit heteromers are apparently stable protein complexes (Sellin et al., 2011a), which is in contrast to the cognate complexes of budding yeasts, in which septin subunits may be exchanged (McMurray and Thorner, 2008). Hydrodynamic parameters and electron microscopy revealed that all mammalian heteromers contain SEPT2 and SEPT6 subgroup members and SEPT7, whereas octamers additionally contain the ubiquitous SEPT9 protein—the sole SEPT3 subgroup member expressed by the cell types used. A subsequent report analyzing the effects of mutations on interactions between specific septins provides further evidence that SEPT9 caps the ends of octameric heteromers by forming a G-interface with SEPT7 (Kim et al., 2011).

Septin localization to the contractile ring during cytokinesis is conserved across kingdoms. In budding yeast, septin hetero-oligomers assemble at the bud neck during interphase of the cell cycle and are visible as distinct rings and gauzes that reorganize during cytokinesis (i.e., septation, hence the name "septins"; for review, see McMurray and Thorner, 2009). In interphase animal cells, however, a variety of septin arrangements are reportedly dispersed in the cortical cytoplasm bound to actin bundles or microtubules. Moreover, cross-talk between septins and microtubules have been reported with proposed relevance for epithelial cell polarization and the function of the mitotic spindle (Spiliotis et al., 2005; Bowen et al., 2011). We recently described the basis for live-cell imaging of native higher-order septin arrangements in human cells using fluorescent reporters (Sellin et al., 2011a). In nonadhered cells, all septin heteromers appear to assemble into uniformly sized, submembranous, disk-like structures, which depend on microtubules for structural integrity. As anticipated from previous studies on substrate-dependent cell types (reviewed in Spiliotis and Gladfelter, 2011), septin disks are transformed into other arrangements in response to microtubule-directed drugs or cell adherence to integrin-activating ligands (Sellin et al., 2011a).

SEPT9 is the only ubiquitously expressed member of the SEPT3 subgroup (SEPT3, SEPT9, and SEPT12), and this septin has been linked to diverse human disorders. Evidence includes a variety of alterations in cancer cells and mutations associated with hereditary neuralgic amyotrophy (reviewed in Beise and Trimble, 2011). The SEPT9 locus is complex, and alternative splicing results in six confirmed protein isoforms with a common G-domain but variable N-terminal extensions (see Figure 1A). RNA interference experiments in epithelial cells lines revealed a role of SEPT9 in midbody abscission (Estey et al., 2010). Moreover, homozygous deletion of Sept9 in mice results in embryonic lethality, and Sept9−/− embryonic fibro-blasts exhibit a twofold to threefold increased frequency of cells with abnormal and/or multiple nuclei (Fuchtbauer et al., 2011).

SEPT9 has been reported to localize to microtubules in epithelial cell lines (Surka et al., 2002; Nagata et al., 2003), but this localization has not been evident from cell images shown in subsequent reports, in which colocalization of SEPT9 with other septins on actin bundles and at cell edges is highlighted (Hanai et al., 2004; Estey et al., 2010). Colocalization of SEPT9 with other septins is as would be predicted by recent findings that SEPT9 is a subunit of octameric heteromers in which all four septin subgroups are represented (Kim et al., 2011; Sellin et al., 2011b). However, previous studies have not considered the heteromeric context and stoichiometry of different SEPT9 isoforms. Here we used a gene product replacement strategy to generate cell lines in which octameric heteromers have either a native or fluorescent-reporter–tagged SEPT9 isoform at their ends. We found that both hexameric and octameric heteromers incorporate into microtubule-supported submembranous septin disks. Although the septin disk arrangement does not depend on SEPT9 per se, an increased abundance of a SEPT9 isoform with a short N-terminal extension causes an increased disk diameter. In contrast, similar expression of the SEPT9 isoform with the longest N-terminal extension facilitates septin heteromer polymerization along interphase microtubules. Our combined evidence points to the significance of tissue-specific SEPT9 isoform composition and the ratio of hexamers to octamers for the higher-order arrangement of septin filaments.

RESULTS

SEPT9 protein isoforms a, b, and f are expressed in the human myeloid K562 cell line

SEPT9 is the only SEPT3-subgroup member expressed by K562 cells (Sellin et al., 2011b). The Consensus Coding Sequence (CCDS) database reports seven confirmed mRNA variants transcribed from the human SEPT9 gene (www.ncbi.nlm.nih.gov/CCDS). These variants, denoted CDS-v1 to -v7 in Figure 1A, encode the six SEPT9 protein isoforms a–f (nomenclature according to the National Center for Biotechnology Information Reference Sequence collection), which differ in both the length and sequence of the N-terminal extension. As depicted in Figure 1A, the coding sequences (CDS) of mRNAs for isoforms a–d include unique 5′-exons, whereas translation of isoforms e and f is initiated at in-frame AUG codons within exons 7 and 10, respectively. As highlighted in Figure 1A, all transcripts encompass the coding region for isoform f, which has a very short N-terminal region before the conserved G-domain. SEPT9 mRNA expression of the present cell model system—a human cell line of hematopoietic origin—was determined by reverse transcription (RT)-PCR. Figure 1B shows that only transcript variants 1 and 2 were detected, which encode the SEPT9(a) and SEPT9(b) isoforms, respectively.

To determine the repertoire of SEPT9 protein isoforms and their dependence on a native heteromeric context, we transfected K562 cells with vectors for RNA interference targeting of SEPT9 (short hairpin RNA[SEPT9] [shRNA[SEPT9]]) or SEPT7 (shRNA[SEPT7]). For this we used episomally replicating vectors with a selectable marker, which allow rapid selection of specifically depleted cell lines. Western analysis of extracts (Figure 1C) shows that antibodies raised against the common C-terminal 320 residues of all SEPT9 proteins detect three bands corresponding to the sizes of isoforms a (~73 kDa), b (~72 kDa), and f (~40 kDa). Note that a faint nonspecific band (~58 kDa, labeled NS) is also visible in SEPT9-depleted cells. As anticipated by detection of transcript variants 1 and 2 by RT-PCR analysis, the cognate SEPT9(a) and SEPT9(b) isoforms represent the major SEPT9 proteins (Figure 1C). The ~40-kDa band, which migrates indistinguishably from a recombinant version of isoform

A

Coding RNA: Exon No.   SEPT9 isoform:

CDS_v1   1 | 3   (586 aa) a

CDS_v2   5   (579 aa) b

CDS_v3   4   (568 aa) c

CDS_v4   9   (474 aa) d

CDS_v5/6   AUG   (422 aa) e
           7

CDS_v7   AUG   (335 aa) f   STOP
         10 | 11 | to | 17 | 18
         <--- G-domain --->

B

SEPT9_: v1   v2   v3   v4   v5   v6   v7
5'-exon: 1   5   4   9   2*   6*   8*

394
344
298
220

C   Vec-Co shRNA^SEPT9 shRNA^SEPT7 rSEPT9(f)   Blot:

         a
         b
67►
NS   SEPT9
43►   f

                                       SEPT7

                                       SEPT2

                                       SEPT6

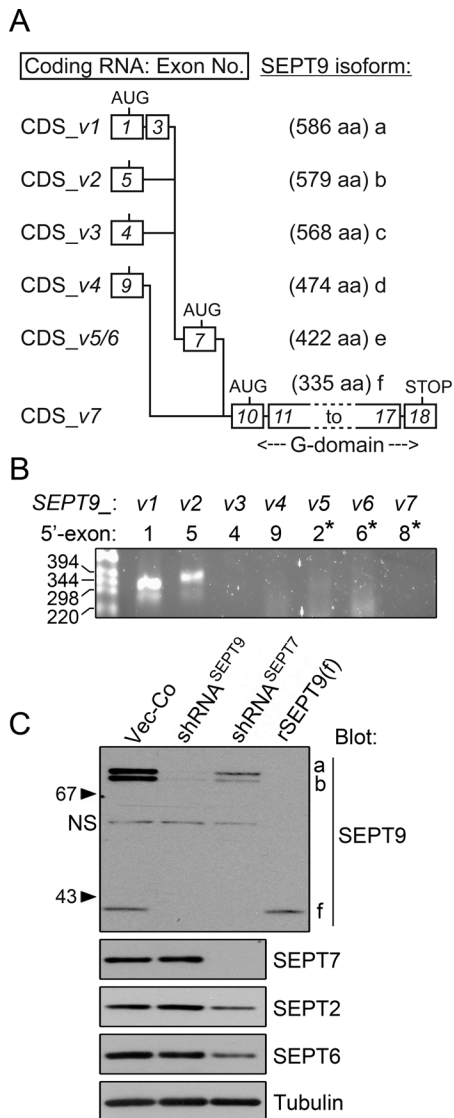   Tubulin

FIGURE 1: *SEPT9* transcript variants and protein isoforms expressed by the K562 cell model system. (A) Splicing of the cognate coding exons into the mRNA coding sequences (CDS) of *SEPT9* transcript variants 1–7 (termed CDS-v1 to CDS-v7). The length (amino acids [aa]) of the cognate protein isoforms (a–f) is indicated. Exons cognate to coding mRNA are depicted as boxes and numbered according to their order in the genome (exons 10–18 are common to all confirmed coding mRNAs). Translation of isoforms e and f starts at in-frame AUG codons of exons 7 and 10, respectively. Exons cognate to 5′-untranslated regions (UTRs) are not depicted (i.e., exons 2, 6, and 8). The data are gathered from National Center for Biotechnology Information and CCDS reference sequences (exons are not drawn to scale). (B) RNA was isolated from K562 cells, and *SEPT9* transcript variants were screened by RT-PCR. The 5′-primers are based on the indicated 5′-exon of each transcript variant. An asterisk indicates exons cognate to 5′-UTRs, which are not depicted in A. Primer pairs and PCR product length (in all cases between 347 and 400 base pairs) are described in the Supplemental Materials and Methods. Two independent primer pairs per mRNA variant were tested. (C) Western blot detection of the indicated septins. K562 cells were transfected with replicating RNA interference vectors directing expression of short hairpin RNAs targeting all mRNA variants of either *SEPT9* (shRNA^SEPT9) or *SEPT7* (shRNA^SEPT7) and counterselected in hygromycin for 1 wk. As a reference, the analysis includes a recombinant version of SEPT9 isoform f (termed rSEPT9(f)) overexpressed by transfected K562 cells. SEPT9 isoforms are

SEPT9(f), is produced at lower levels. Given that only transcript variants 1 and 2 are detected by RT-PCR (Figure 1B), these results suggest that the SEPT9(f) isoform is generated by alternative translational initiation within the longer transcript(s). The estimated ratio of SEPT9 isoforms a, b, and f in K562 cells is 2:2:1, respectively.

Most mammalian septins are aggregation prone and/or unstable if expressed without appropriate hetero-oligomerization partners (Kinoshita, 2003; Sheffield *et al.*, 2003; Sellin *et al.*, 2011b). Moreover, depletion of SEPT7—the obligatory subunit of all native heteromers— decreases the cell content of other septins (Kinoshita *et al.*, 2002; Estey *et al.*, 2010). We recently reported that all the septins expressed by K562 cells depend on SEPT7 for their stability (Sellin *et al.*, 2011b). Figure 1C shows the effect of SEPT7 depletion on SEPT9 isoforms. Quantification of Western blots suggests that SEPT7 depletion reduces all three SEPT9 isoforms, as well as SEPT6 and SEPT2, to a similar extent, with the residual levels corresponding to ~20% of those in control cells. Thus, when expressed at endogenous levels, the stability of SEPT9 isoforms appears equally dependent on assembly into SEPT7-containing core heteromers.

All of the endogenous SEPT9 isoforms appear equally represented in higher-order septin structures in interphase K562 cells

The only distinctive higher-order septin arrangement observed in nonadhered K562 cells during interphase are uniformly sized submembranous structures termed septin disks, which disassemble upon permeabilization of cells at physiological ionic strength (Sellin *et al.*, 2011a). To estimate the fraction of each SEPT9 isoform that is incorporated into these septin disks, we permeabilized K562 cells by saponin at a low ionic strength. Soluble proteins were then separated from the insoluble particulate cell fraction by centrifugation, with partitioning between these two fractions monitored by Western blotting. Figure 2A shows the expected release of the cytosolic marker protein Oncoprotein 18/Stathmin (Op18) into the supernatant (S) and retention of the intermediate filament protein vimentin in the pellet (P) after permeabilization at both near-physiological (1× PEM buffer [80 mM 1,4-piperazinediethanesulfonic acid [PIPES], pH 6.9, 2 mM MgCl$_2$, 4 mM ethylene glycol tetraacetic acid]) and decreased (0.25× PEM) ionic strength. In contrast, all three SEPT9 isoforms are released after permeabilization in 1× PEM, whereas a major fraction of each isoform is retained by cells permeabilized under decreased–ionic strength conditions (0.25× PEM).

The results in Figure 2A do not indicate any differences in the partitioning of SEPT9 isoforms a, b, and f. Moreover, the partitioning of SEPT9, SEPT2, SEPT6, and SEPT7 using graded PEM buffer dilutions shows that that their partitioning profiles are indistinguishable (Figure 2B). These results are consistent with the notion that the SEPT9 isoforms and other septins expressed by K562 cells are all combined into the main interphase arrangement of this cell type, namely septin disks.

Expression of *Aequorea coerulescens* green fluorescent protein–SEPT9 isoform reporters decreases the levels of all of the endogenous SEPT9 isoforms

Newly synthesized SEPT2, SEPT6, or SEPT7 is not detectably incorporated into preexisting heteromers, indicating that mammalian

indicated at the right top (left, nonspecific [NS]). and tubulin is used as loading control. Serial dilution of cell extracts indicated that SEPT9(f) constitute ~20% of the total SEPT9 proteins in K562 cells. Data are representative of three independent transfection experiments.
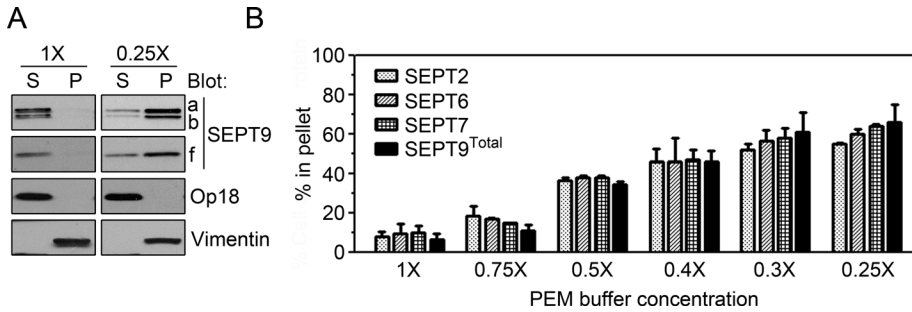
FIGURE 2: Partitioning of individual septins between soluble and insoluble fractions of cells permeabilized at graded ionic strengths. (A) K562 cells were permeabilized by saponin (0.2%) in either 1× PEM or 0.25× PEM buffer. The released (supernatant [S]) and cell-associated (pellet [P]) proteins were analyzed by Western blot using the indicated antibodies. The release of a cytosolic protein (Op18) and retention of the intermediate filament protein vimentin served as a marker for cell permeabilization. (B) The fraction of the indicated septins within cell pellets after saponin (0.2%) permeabilization with the indicated PEM buffer concentration was determined by quantification of Western blots. SEPT9[total] represents all three endogenous isoforms, which appeared indistinguishable with respect to their partitioning. Bar charts represent the mean ± errors of data from duplicate experiments.
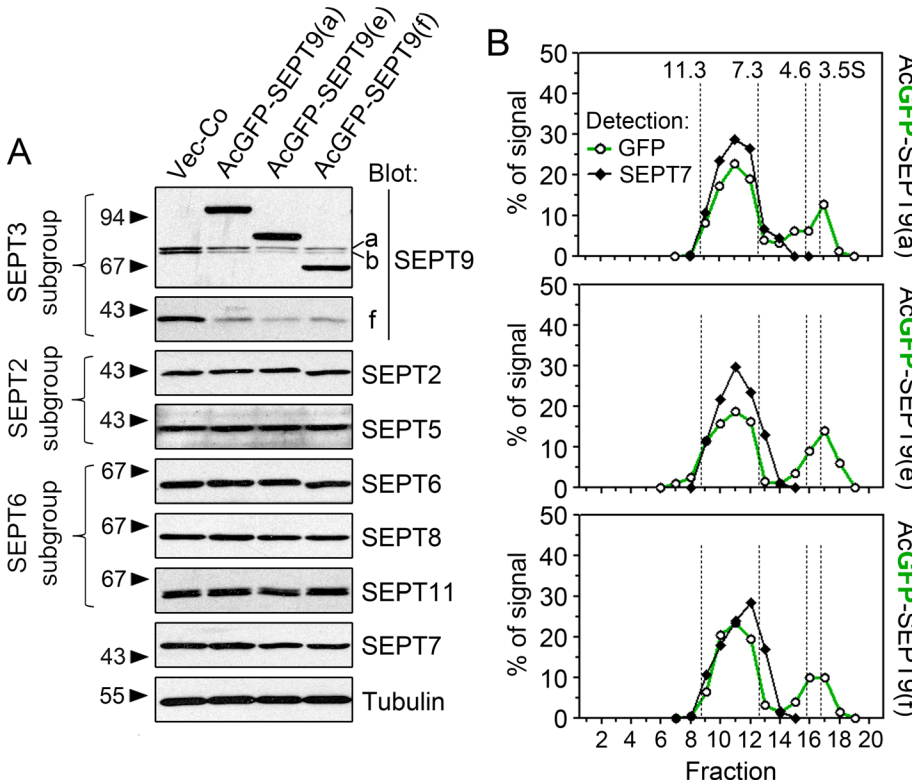

FIGURE 3: Analysis of endogenous septins and hetero-oligomerization in cell lines expressing AcGFP-tagged SEPT9 isoform reporters. K562 cells were transfected with pMEP-based, episomally replicating vectors directing regulatable expression of the indicated SEPT9 derivative. Cells were counterselected with hygromycin, and expression was controlled as outlined in *Materials and Methods*. (A) Western blot detection of septins expressed by K562 cells. Septins belonging to the SEPT2, SEPT3, and SEPT6 homology-based subgroups are indicated at the left margin. (B) Crude extract of cells transfected with the indicated AcGFP-SEPT9 isoform was analyzed by density-gradient centrifugation. Transfection conditions were adjusted for modest expression levels, which correspond to ~50% of the level in A. The distribution of heteromers (detection based on SEPT7) and AcGFP-SEPT9 was analyzed by Western blotting. Note that six- and eight-subunit heteromers are not resolved by this method and that a 26.9-kDa AcGFP-fusion partner is too small to detectably alter sedimentation profiles. Sedimentation peaks for proteins of known S values are indicated by vertical dotted lines.

core heteromers are essentially stable protein complexes (Sellin *et al.*, 2011a). Although overexpression of individual septin subunits does not appear to alter the content of SEPT7-containing core heteromers, we found that unbalanced expression results in ectopic filaments, aggregates, and/or homology subgroup–restricted degradation of endogenous septins (Sellin *et al.*, 2011b). The combined evidence in these previous reports suggested homology subgroup–directed assembly of core heteromers and that septin subunits may compete for limiting amounts of stabilizing heterooligomerization partners.

To address how overexpression of specific SEPT9 isoforms may affect the level of endogenous septins, we used episomally replicating vectors that enable regulatable expression and rapid selection of transfected cell lines. We included SEPT9 isoforms a, e, and f in this analysis because 1) K562 expresses SEPT9(a) and SEPT9(f), and 2) all confirmed SEPT9 transcript variants except CDS-v7 contain the open reading frame encoding SEPT9(e) (see Figure 1). For detection, an *A. coerulescens* green fluorescent protein (AcGFP) fluorescent reporter was fused to the N-terminal end, which varies among isoforms, because fusion to the C-terminal of SEPT9 blocks assembly into core heteromers (Sellin *et al.*, 2011a). Figure 3A shows how expression of these AcGFP-tagged SEPT9 isoforms affects the endogenous K562 septins. The data show that expression of each of these proteins results in a similar decrease of all the endogenous SEPT9 isoforms while leaving the levels of all other septins unaffected. Because SEPT9 is the only SEPT3 subgroup member expressed in K562 cells, the data are consistent with subgroup-restricted competition for stabilizing heterooligomerization partners (Sellin *et al.*, 2011b).

Next we examined the heteromeric context of AcGFP-tagged SEPT9 proteins when expressed at moderate levels (~50% of the levels in Figure 3A) by density gradient centrifugation. As anticipated by their competition with endogenous SEPT9 isoforms (as shown in Figure 3A), a major fraction of the AcGFP-SEPT9 isoforms sediment as a single peak coinciding with SEPT7-containing heteromers (Figure 3B; note that hexameric and octameric heteromers are not resolved by this method; Sellin *et al.*, 2011b). Thus all of the AcGFP-SEPT9 isoform reporters appear to be capable of effectively assembling into the pool of septin core heteromers.
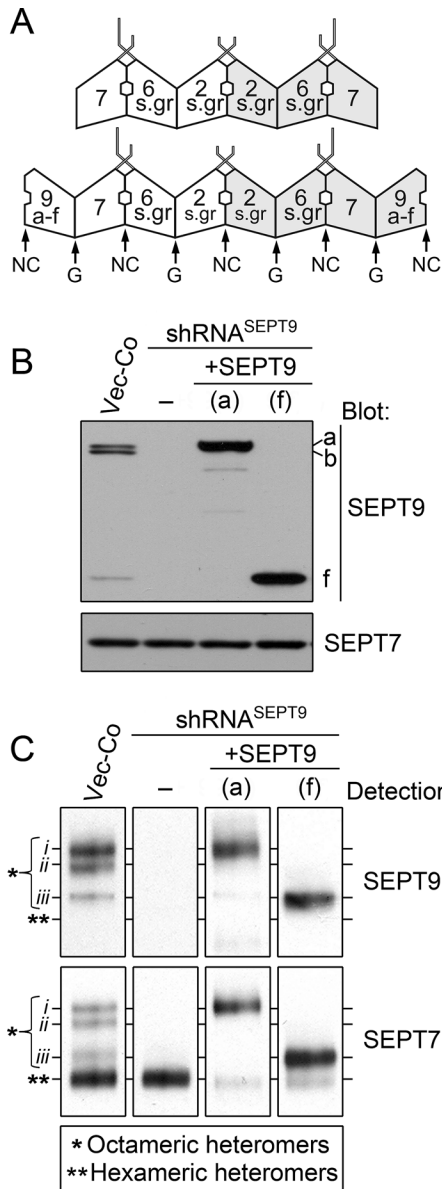
FIGURE 4: Analysis of septin heteromer size distributions by Blue native PAGE in control and genetically manipulated K562 cells. (A) Depiction of the repertoire of hexameric and octameric core heteromers in K562 cells. The arrangement of SEPT2-subgroup (2-s. gr) and SEPT6-subgroup (6-s.gr) members, as well as of SEPT7, is according to the solved structure of a recombinant head-to-head SEPT2/6/7 trimer (PDB ID 2qag; shaded areas indicate different faces of trimeric and tetrameric units). Octamers are depicted with any of the SEPT9 isoforms a–f at their ends (modified from Sellin et al., 2011b). However, whereas SEPT3-subgroup members differ in the N-terminal extensions, the G-domain is highly homologous (Cao et al., 2007). Thus it seems likely that SEPT3, SEPT9, and SEPT12 are exchangeable subunits at the tips of octameric septin heteromers. (B) K562 cells were transfected with empty vector (Vector-Co) or the replicating RNA interference vector shRNA[SEPT9] or cotransfected with shRNA[SEPT9] and the indicated pMEP-SEPT9 derivative, which contains silent mutations within the shRNA[SEPT9]-targeted sequence. Cells were counterselected with hygromycin, and expression was controlled as outlined in *Materials and Methods*. The native open reading frames of SEPT9(a) and SEPT9(f) were expressed from the hMTIIa promoter using the same conditions as in Figure 3B. Expression levels of SEPT9 isoforms and SEPT7 were analyzed by Western blotting. (C) Septin heteromers were resolved by Blue native PAGE and transferred to polyvinylidene fluoride filters for immunodetection of SEPT9-containing (top) and SEPT7-containing (bottom) heteromers. Complexes in Vector-Co cells corresponding to octameric heteromers (*) are denoted i–iii. The position of hexameric heteromers is indicated by double asterisks. The data are representative for at least three independent experiments.

The expression level of SEPT9 isoforms directs the ratio of octameric to hexameric septin heteromers

Recent evidence supports the model depicted in Figure 4A, in which hexamers and octamers are arranged according to homology subgroups. Single-particle analysis indicates that octamers comprise ~40% of all heteromers in K562 cells and suggests a cooperative hetero-oligomerization mechanism by which octamers, but not heptamers, are generated under conditions of limiting amounts of SEPT9 (Sellin et al., 2011b).

To address whether elevated SEPT9 expression increases the fraction of octameric heteromers, we used a gene replacement strategy in which single SEPT9 isoforms are expressed in cells depleted of endogenous SEPT9 isoforms. Our genetic system involved expression of individual *SEPT9* isoforms from replicating pMEP4 expression plasmids carrying silent point mutations that render them immune to RNA interference by the shRNA[SEPT9] plasmid used to deplete the endogenous gene products. Western blots in Figure 4B confirm SEPT9 depletion by RNA interference, as well as expression of the single SEPT9(a) and SEPT9(f) isoforms at threefold to fivefold higher levels than the total content of endogenous SEPT9 isoforms in control cells.

Because density gradient centrifugation or gel-filtration chromatography does not resolve hexameric and octameric heteromers (Figure 3B; Sellin et al., 2011b), we optimized conditions for resolving heteromer subpopulations by Blue native PAGE electrophoresis. This technique preserves large protein complexes and provides high-resolution separation based on molecular mass and shape (Wittig et al., 2006). Figure 4C shows immunodetection of SEPT9- and SEPT7-containing heteromers separated by this method. Anti-SEPT9 reveals three complexes (denoted i–iii) in control K562 cells (Vector-Co), all of which are absent when endogenous SEPT9 is depleted via shRNA[SEPT9] expression. In contrast, four SEPT7-containing complexes are resolved in control cells, but only the lower complex is detected upon SEPT9 depletion (i.e., in shRNA[SEPT9]-expressing cells). The three complexes detected by anti-SEPT9 in control cells migrate indistinguishably from the three upper complexes detected by anti-SEPT7, which predictably detects all heteromers. Hence the lower complex detected by anti-SEPT7 in control cells corresponds to hexameric heteromers that lack SEPT9 subunits. Quantification by serial dilutions of these cell extracts suggests that octameric heteromers (i.e., the sum of complex i–iii) comprise ~40% of all heteromers detected by anti-SEPT7, which agrees with estimates based on electron microscopy (Sellin et al., 2011b).

Figure 4C also shows Blue native PAGE separation of heteromers of cells in which endogenous SEPT9 isoforms are replaced by either the SEPT9(a) or SEPT9(f) isoform. It is evident from these data that an overall increase in the SEPT9 content (three to fivefold; see Western blots in Figure 4B) results in a diminishing fraction of hexameric heteromers. Thus these results establish that SEPT9 expression levels direct the octamer-to-hexamer ratio in K562 cells.

Expression of SEPT9(a) or SEPT9(f) at adequate levels generates a single major complex migrating indistinguishably from complex i or iii, respectively (Figure 4C), which is consistent with control K562 cells expressing these isoforms. In the Supplemental Material we detail the evidence suggesting that the octamer designated
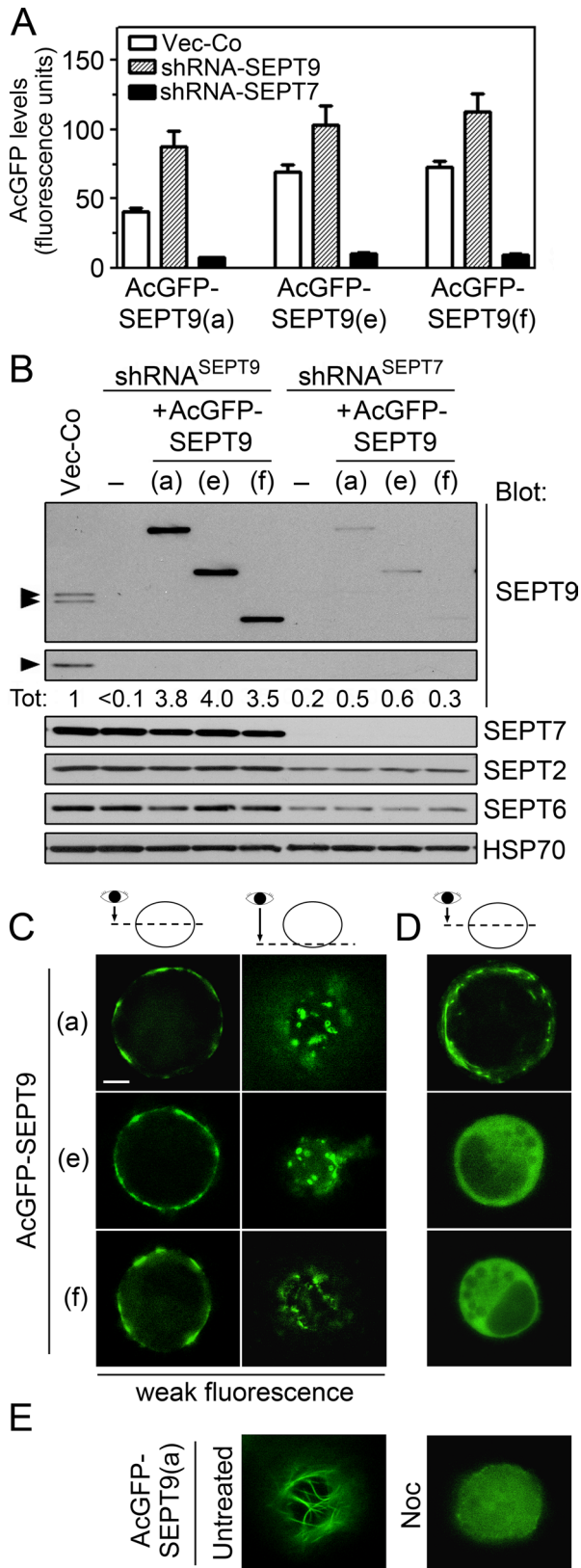
FIGURE 5: The localization of octameric heteromers tagged with a single AcGFP-SEPT9 isoform at their ends. (A) Cells were cotransfected with the indicated pMEP-AcGFP-SEPT9 derivative (AcGFP fused to the N-terminus) combined with Vector-Co (open bars) or the replicating RNA interference vector shRNA^SEPT9 (shaded bars) or shRNA^SEPT7 (filled bars). The expressed SEPT9 derivatives contain

i contains either SEPT9(a) or the similarly sized SEPT9(b), that the octamer designated *iii* contains SEPT9(f) only, and that the one designated *ii* contain SEPT9(a) or SEPT9(b) at one end and SEPT9(f) at the other end (Supplemental Figure S1). It is notable that the present data give no indication of heptamers in control or SEPT9-overexpressing cells, which suggests cooperativity during octamer assembly.

The SEPT9(a) isoform confers microtubule association in cells containing a predominantly octameric heteromer pool

We used the aforementioned genetic system to replace the endogenous SEPT9 isoforms with individual AcGFP-tagged isoforms. The transfection conditions used were the same as in Figures 3B and 4, which had been attuned to generate a predominantly octameric pool combined with minimal accumulation of monomeric AcGFP-SEPT9. The consequences of depleting either SEPT7 or SEPT9 for the stability of AcGFP-SEPT9 reporters were initially evaluated by analysis of the AcGFP fluorescence intensities of transfected cell lines. Flow cytometry of live cells (Figure 5A) showed that depletion of endogenous SEPT9 increased the cellular content of AcGFP-SEPT9 reporter proteins by 1.5- to 2-fold, as would be predicted by a decreased competition for stabilizing hetero-oligomerization partners. Furthermore, analysis of SEPT7-depleted cells revealed that stability of the AcGFP-SEPT9 proteins is highly dependent on assembly into SEPT7-containing heteromers.

As estimated by quantitative Western blotting in Figure 5B, the amount of each AcGFP-SEPT9 protein in cell lines depleted of endogenous SEPT9 is approximately fourfold higher than the sum of the endogenous SEPT9 isoforms in control cells, that is, an expression level that should be sufficient to attain a predominantly octameric pool of heteromers. The data shown in Figure 5B also confirm that depletion of SEPT7 destabilizes each of the AcGFP-SEPT9 isoforms, as well as endogenous septins. Thus the genetic system appears appropriately attuned to attain both efficiency and specificity in AcGFP tagging of octameric septin heteromers.

Blue native PAGE analysis showed that expression of each of the AcGFP-SEPT9 isoforms results in uniformly sized octamers in which the presence of AcGFP is identifiable by a shift in mobility (Supplemental Figure S1). This analysis also revealed a residual pool of

silent mutations within the shRNA^SEPT9-targeted sequence, and conditions were adjusted for modest expression levels (same as Figure 3C; see *Materials and Methods*). Expression levels of AcGFP-tagged SEPT9 were determined by flow cytometry of live cells. (B) Western blot detection of the indicated septins in crude extracts of cotransfected cells described in A (Hsp70: loading control). The relative SEPT9-content (Tot) was determined by Western blotting of serially diluted extracts. The sum of the endogenous isoforms in Vector-Co cells is set as 1. (C–E) Epifluorescence microscopy of live cells in which the endogenous SEPT9 isoforms were replaced with the indicated AcGFP-SEPT9 isoform reporter by the gene product replacement strategy described in A (i.e., cotransfection of shRNA^SEPT9 and shRNA-immune pMEP-AcGFP-SEPT9 derivatives). (C) Representative weakly fluorescent cells, which represent <10% of the cell population. (D, E) Representatives of the majority of cells, which are brightly fluorescent (the distribution of fluorescence intensity is shown in Supplemental Figure S1). (E) Right, the effect of nocodazole-mediated microtubule depolymerization (Noc, 6 μM for 30 min) on a brightly fluorescent AcGFP-SEPT9(a)–expressing cell. The results are representative for two independent AcGFP-SEPT9 isoform–expressing K562 cell lines. The images represent deconvoluted optical sections at the equatorial plane (C, D), parallel to the plasma membrane (C), or below the nucleus (E). Scale bar, 5 μm.

hexamers, which would be anticipated due to varying AcGFP-SEPT9 expression within the cell population (Supplemental Figure S2). The absence of endogenous SEPT9 implies that the fluorescence intensity can be expected to correlate with the octamer-to-hexamer ratio in individual cells. This is an essential premise for interpretations of cell images presented in Figure 5, C–E, which shows optical sections at the cell equator and parallel to the plasma membrane (note that K562 are spherical cells that grow independently of an adhesion substrate). Thus, in the minority of cells in which the octamer-to-hexamer ratio is predictably low (i.e., weak AcGFP-fluorescence; Figure 5C), all three AcGFP-SEPT9 isoforms visualized cortical punctuate assemblies, which were not observed among the majority of cells that are brightly fluorescent (Figure 5, D and E). Albeit less distinct in appearance, these assemblies resemble the previously identified submembranous septin disks (Sellin et al., 2011a), which are further characterized later (see later discussion of Figure 9).

The observed octamer-to-hexamer ratio (Supplemental Figure S1) predicts that the majority of cells, which are brightly fluorescent, have heteromer pools that primarily consist of AcGFP-tagged octamers. As shown in Figure 5D, both the AcGFP-SEPT9(e) and AcGFP-SEPT9(f) isoform reporters were nonlocalized in the cytosol of these cells, whereas elongated structures were observed in AcGFP-SEPT9(a)–expressing cells. Optical sections parallel to the plasma membrane show that the AcGFP-SEPT9(a) isoform visualizes filaments that appear as microtubules (Figure 5E, left; a section below the nucleus is shown). These filaments are disrupted by microtubule depolymerization, which results in nonlocalized fluorescence (Figure 5E, right, 30 min with nocodazole). Thus, whereas AcGFP-SEPT9(a)–tagged octamers assemble into septin disk-like structures in weakly fluorescent cells, an apparent microtubule association is evident in the majority of cells.

As evidenced in following sections, the nondistinct appearance of septin disks, as well as the examples of diffuse cytosolic localization, can be attributed to the AcGFP-fusion partner, which in certain cases interferes with heteromer assembly. Nevertheless, AcGFP tagging of the SEPT9(a) isoform revealed octamer association to interphase microtubules and that this property requires a high octamer-to-hexamer ratio. These results, combined with previous evidence that a monomeric SEPT9(a)-AcGFP reporter derivative is nonlocalized in K562 cells (Sellin et al., 2011a), suggest that microtubule association requires cooperation between SEPT9(a)-containing octamers.

Taxol-mediated bundling is required for stable microtubule association of the native pool of octameric and hexameric heteromers in K562 cells

Treatment of cells with low concentrations of Taxol stabilizes microtubules in their native state, but high concentrations of this drug result in a gradual accumulation of microtubules bundles. To address the significance of microtubule bundling for septin interactions, we exposed briefly cells (3 min) to graded concentrations of either nocodazole or Taxol and subsequently permeabilized them in a buffer that preserves the polymerization state of microtubules. Western blotting of soluble and particulate proteins was used to determine whether the fraction of polymeric tubulin correlated with retention of septins by permeabilized cells.

Figure 6A depicts the dose responses of nocodazole-mediated depolymerization and Taxol-mediated increased polymerization in relation to untreated cells that contain ~40% particulate (i.e., polymeric) tubulin (dotted line). The results revealed that detectable retention of septins require >0.2 μM Taxol, that is, conditions promoting essentially complete polymerization of tubulin. It should be noted that although K562 cells express the SEPT9(a)
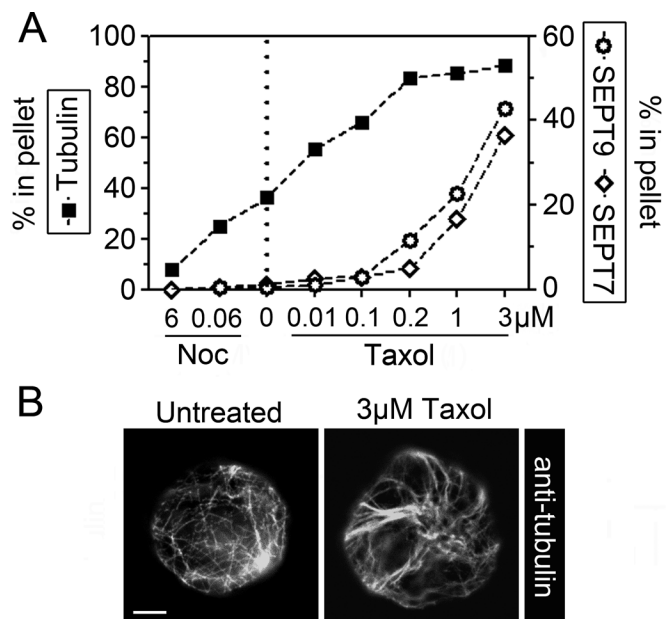

FIGURE 6: Microtubule-dependent retention of septins in permeabilized cells. (A) K562 cells were treated for 3 min with graded concentration of either nocodazole (6 and 0.06 μM) or Taxol (0.01, 0.1, 0.2, 1, and 3 μM) and subsequently permeabilized at 37°C by saponin in a microtubule-stabilizing buffer. The released vs. pelleted protomer entities of either microtubule (α-tubulin) or septin heteromers (SEPT7 and SEPT9) were quantified by Western blotting as in Figure 2B. The data are expressed as percentage polymeric tubulin at various drug concentrations (untreated cells, marked by a dotted line) vs. the fraction of cell-associated SEPT7 or SEPT9 (with SEPT9 indicating the sum of the three expressed isoforms). (B) The appearance of microtubules of fixed cells that are either untreated (top) or treated for 3 min with 3 μM Taxol (bottom). Scale bar, 5 μm.

isoform and octamers comprise only ~40% of the heteromer pool (see Figures 1C and 4C), retention of SEPT7 and SEPT9 coincided at all Taxol concentrations. In addition, Western blots did not reveal differences among SEPT9 isoforms (unpublished data). Thus the present analysis does not distinguish any particular subpopulation of septin heteromers but suggests a significance of microtubule bundling.

Immunofluorescence of cells treated with 3 μM Taxol did not reveal any large microtubule bundles within the first hour. However, the general appearance is still altered within some minutes such that microtubules extending along the cell cortex appear as thin bundles (Figure 6B). Thus it seems reasonable to assume that the stable microtubule association of the native septin heteromer pool of K562 cells shown in Figure 6A depends on Taxol-promoted bundling. This is consistent with reports describing a propensity of septins to associates to bundled, but not individual, microtubules (Martinez et al., 2006; Bowen et al., 2011; Sellin et al., 2011a).

A heteromer pool consisting primarily of SEPT9(a) isoform–containing octamers is stably associated with nonbundled microtubules

To analyze SEPT9-dependent microtubule interactions of authentic octameric heteromers, we generated cell lines in which the endogenous isoforms were replaced with single isoforms expressed from their native open reading frames. We used the same conditions as in Figure 4, which were shown previously to result in a predominant octameric heteromer pool. Western blots in
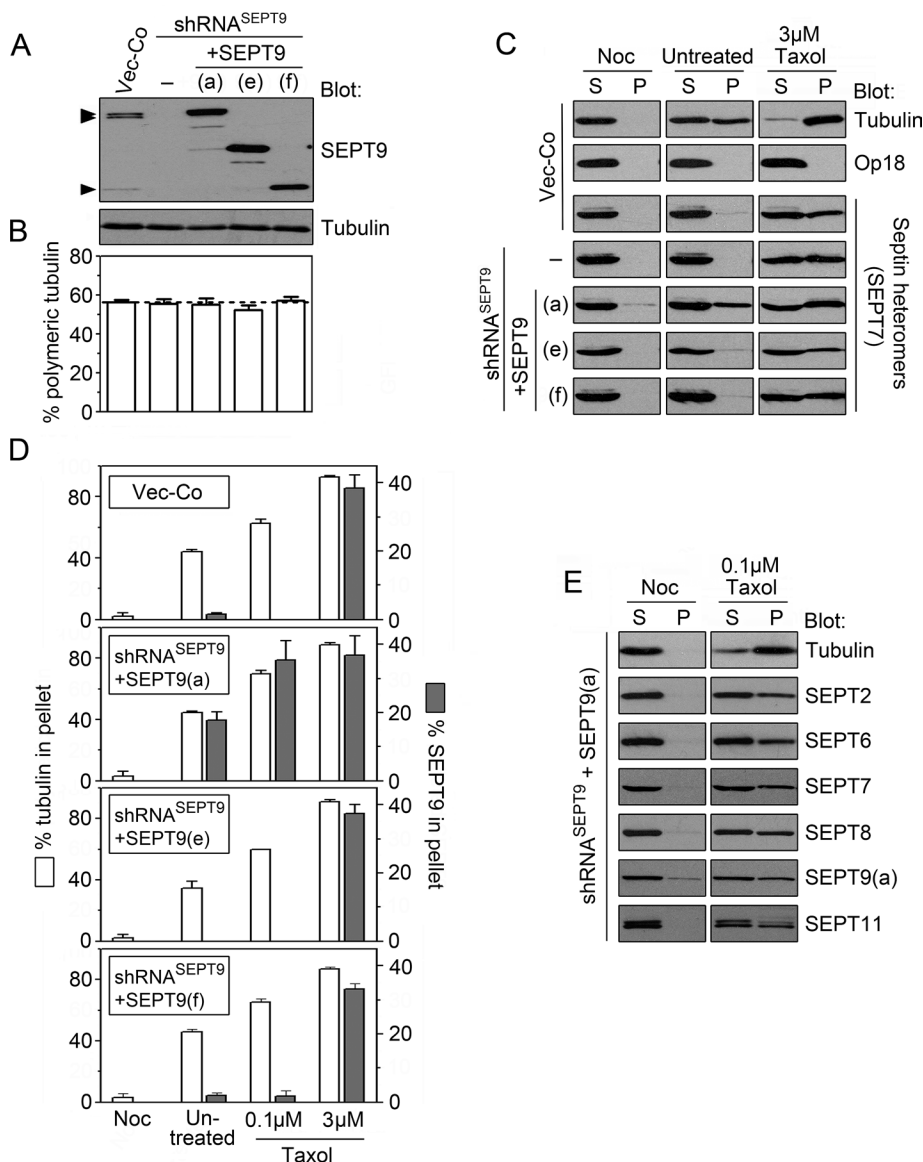
FIGURE 7: Characterization of cell lines in which the three endogenous SEPT9 isoforms are replaced with a single native isoform expressed at levels that generate a predominately octameric heteromer pool. Cells were cotransfected with the indicated pMEP-SEPT9 isoform derivative (native open reading frame) combined with vector control or a shRNA^{SEPT9}-expressing vector (same general strategy as in Figures 4 and 5 using shRNA-immune *SEPT9* derivatives). (A) Western blots of SEPT9 and tubulin in crude extracts of cotransfected cells. (B) The total content of microtubules was determined as outlined in *Materials and Methods* and expressed as the percentage of polymerization-competent tubulin. (C) Cell lines described in A were treated for 3 min with nocodazole (3 μM, Noc) or Taxol (3 μM, Tax) or left untreated. Cells were subsequently permeabilized at 37°C by saponin in a microtubule-stabilizing buffer. The released (supernatant [S]) and cell-associated (Pellet [P]) proteins were analyzed by Western blot. Tubulin serves as a marker for microtubule stability and SEPT7 as a marker for the partitioning of septin heteromers. Complete release of Op18 indicates efficient cell permeabilization. (D) The partitioning of tubulin and SEPT9 after permeabilization of cells (pretreatment as indicated) was determined by quantification of Western blots. A fraction of the overexpressed SEPT9 isoforms (5–10%) was found in insoluble aggregates, which is subtracted from the presented data. (E) SEPT9(a) isoform–expressing cells were pretreated with nocodazole (3 μM) or Taxol (0.1 μM, i.e., nonbundling conditions). Cells were permeabilized, and the partitioning of the indicated septins was analyzed by Western blotting as in C. The minor residual SEPT9(a) found in the pellet of nocodazole-treated cells is due to aggregates of the overexpressed protein.

Figure 7A confirmed efficient SEPT9 replacement and expression of ectopic SEPT9 isoforms at severalfold higher levels than the endogenous SEPT9 isoforms. Figure 7B shows that the microtubule content is not detectably altered in any of these cell lines, suggesting that these manipulations of the SEPT9 isoform composition do not significantly alter microtubule stability.

To address SEPT9 isoform-specific properties in cells containing octamers with native SEPT9 at their ends, we analyzed microtubule-dependent retention by permeabilized cells using the same conditions as in Figure 6A. Western blots of untreated Vector-Co cells (Figure 7C) demonstrate that permeabilization in a buffer that preserves the native microtubule system results in roughly equal amounts of tubulin in the released (supernatant [S]) and retained (pellet [P]) fractions. As anticipated, 3 min of pretreatment with nocodazole results in complete release, whereas a high Taxol concentration results in complete retention of tubulin. These data confirm efficient depolymerization and hyperpolymerization of microtubules by these drugs, whereas analysis of Op18 demonstrates complete release of soluble cytosolic marker proteins under all conditions.

To estimate retention of septin heteromers by permeabilized cells, we probed Western blots for the SEPT7 subunit common to all heteromers. Consistent with the data presented in Figure 6A, Figure 7C shows that heteromers in Vector-Co cells are only retained under microtubule-bundling conditions (i.e., 3 μM Taxol), and furthermore, that an absence of the endogenous SEPT9 isoforms—or their replacement with the SEPT9(e) or SEPT9(f) isoforms— has no detectable effects. However, in marked contrast, we found that replacement with SEPT9(a) results in retention of SEPT7 even in the absence of Taxol. Thus the data suggest that SEPT9(a), but not the other SEPT9 isoform, confers stable septin heteromer association on the native microtubule system.

The fraction of tubulin heterodimers retained by permeabilized cells is diagnostic for the overall stability of microtubules. Consistent with the data in Figure 7B, quantification of Western blot signals of soluble and retained tubulin suggests that none of the overexpressed SEPT9 isoforms exert significant microtubule stabilizing/destabilizing effects under the four conditions tested (Figure 7D). Furthermore, as anticipated from analysis of endogenous SEPT7 (Figure 7C), we found that SEPT9(a) is always retained in cells, except when microtubules

are depolymerized by nocodazole. Moreover, in cells expressing the SEPT9(a) isoform we found that all other endogenous septins analyzed appear equally represented in heteromers retained by nonbundled microtubules (Figure 7E; note that pellets of nocodazole treated cells contain some SEPT9(a) aggregates, which are subtracted from the data in Figure 7D).

The combined results presented in Figure 7 shows that in cells containing a predominant pool of SEPT9(a) isoform–containing octamers, septin heteromers are stably associated to nonbundled microtubules. Furthermore, the comparison with short SEPT9 isoforms unmasks a strict dependence on the N-terminal extension of SEPT9(a) for this property.

Tracing of octameric heteromers with defined SEPT9 isoforms at their ends by means of low-level SEPT7-AcGFP reporter expression

Replacement of endogenous SEPT7 by a SEPT7-AcGFP reporter was shown to allow visualization of the native septin heteromer arrangements in live cells (Sellin et al., 2011a). Therefore, to trace octameric heteromers with defined subunits at their ends, we combined SEPT9 gene product replacement with SEPT7-AcGFP expression. In these experiments we used transfection conditions as in Figures 4 and 7, which result in a predominantly octameric heteromer pool. In addition, we aimed for substoichiometric SEPT7-AcGFP levels, that is, conditions that allow a low degree of replacement of endogenous SEPT7 that is still sufficient for robust detection through fluorescence. Under these conditions, SEPT7-AcGFP is efficiently assembled into heteromers without the appearance of nonheteromeric SEPT7 or detectable alterations of other septins (Sellin et al., 2011a). The data shown in Figure 8A confirm that expression of the SEPT7-AcGFP reporter is kept sufficiently low as not to cause a significant decrease of endogenous SEPT7, which implies <25% replacement of endogenous SEPT7. These Western blots also confirm efficient depletion of all three endogenous SEPT9 isoforms, as well as their replacement by approximately threefold to fourfold higher levels of a single SEPT9 isoform.

Because SEPT7 is an obligatory subunit of both hexameric and octameric heteromers (see Figure 4A), it can be assumed that the SEPT7-AcGFP protein reports hexamers in cells lacking SEPT9 but is primarily assembled into octamers in cells expressing single SEPT9 isoforms. To characterize the present system for AcGFP tagging of heteromer pools, we analyzed microtubule-dependent retention of SEPT7-AcGFP by the same strategy as in Figure 6 and 7. However, to facilitate detection of stable interactions, we adjusted the permeabilization protocol to decrease heteromer retention in Vector-Co cells (as described in Materials and Methods). In addition, the fraction of retained SEPT7-AcGFP was also determined by flow cytometry prior and subsequent to permeabilization. Figure 8B shows the effects on heteromer retention caused by pretreatment of cells with nocodazole or Taxol at concentrations that mediate depolymerization, stabilization, or bundling of microtubules, respectively. It is evident from the data in Figure 8B that SEPT9(a), but not the shorter SEPT9(e) and SEPT9(f) isoforms, confers a great increase in microtubule-dependent septin heteromer retention by permeabilized cells.

A comparison with the corresponding analyses of native SEPT9 isoforms presented in a previous section (compare Figures 7D and 8B) highlights the effects of an increased ionic strength and incubation time on heteromer retention in detecting the superior stability of SEPT9(a)-conferred septin retention, which is entirely independent on microtubule bundling.
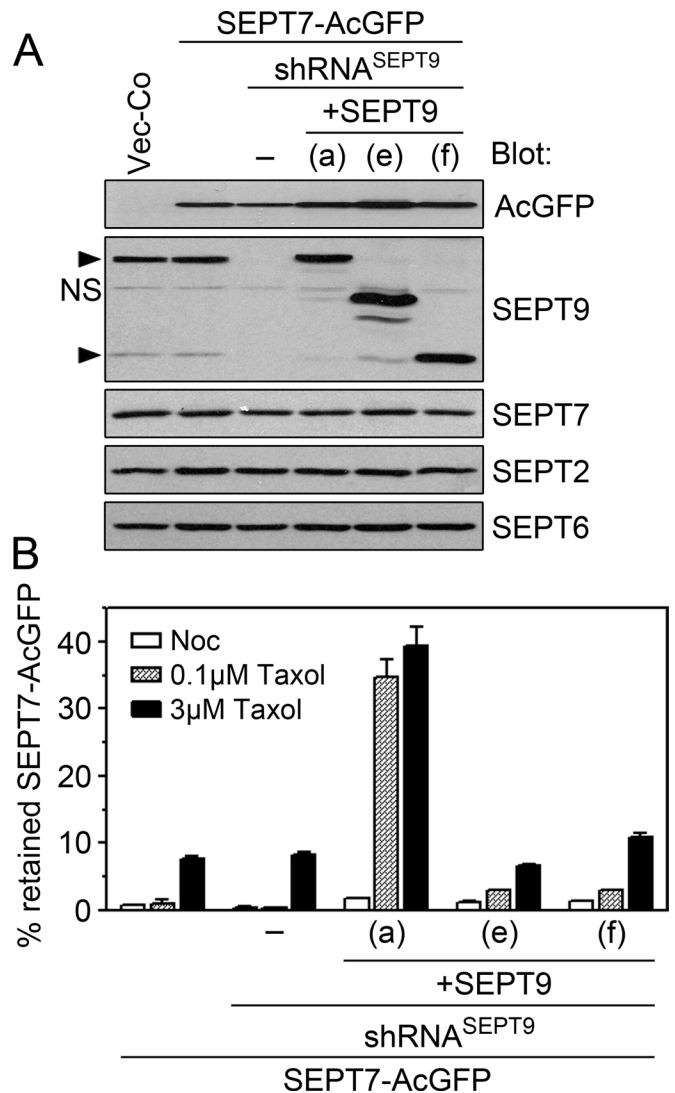

FIGURE 8: Tracing octameric heteromers with a single native SEPT9 isoform at their ends by means of low-level expression of the SEPT7-AcGFP reporter. Cells were cotransfected with the indicated pMEP-SEPT9 isoform derivative, pMEP-SEPT7-AcGFP, and a shRNA^SEPT9 vector (same general protocol as in Figure 7). (A) Western blots of the indicated septins and AcGFP in crude extracts of cotransfected cells. (B) Cells were pretreated for 3 min with nocodazole (3 µM, open bars) or Taxol (0.1 µM, shaded bars; 3 µM, filled bars). The mean fluorescence intensity was determined by flow cytometry prior (total) and post permeabilization (i.e., retained within cells) using stringent conditions as in Figure 6C. Data are expressed as the percentage of AcGFP-SEPT9 retained by permeabilized cells. Data are representative for two independently generated transfected cell lines, which were analyzed on different occasions.

SEPT9 isoforms direct differential microtubule-dependent septin arrangements in cells with heteromer pools consisting primarily of octamers

The genetic system described in the preceding section was also used to visualize how expression of individual SEPT9 isoforms modulates septin arrangements in live cells. Figure 9A shows the localization of the SEPT7-AcGFP reporter in Vector-Co and SEPT9-depleted cells, which in both cases revealed plasma membrane–attached circular structures. We previously termed these septin disks; they are characteristically attached flat against the plasma

membrane, and their integrity depends on intact microtubules (Sellin *et al.*, 2011a). This is the only distinctive higher-order septin arrangement observed in nonadhered K562 during interphase of the cell cycle. Septin disks are evenly distributed around the cortex of the spherical K562 cells and often have a discernible central clearing (see enlargement in Figure 9A of an optical section parallel to the plasma membrane). Expression of shRNA[SEPT9], which decreases SEPT9 by >90% (see Figure 5B), did not alter the general appearance of septin disks. However, the size distribution was altered such that the fraction of small disks is increased (Figure 9B).

Figure 9C shows septin localization in cells with a heteromer pool consisting primarily of SEPT9(a) isoform–containing octamers (optical sections at the cell equator and close to the cell cortex are shown). These cells contain elongated septin filaments, which are disrupted by the microtubule-depolymerizing drug nocodazole (compare top and bottom). The microtubule-like appearance of these filaments is evident in an optical section below the nucleus. It is notable that the filamentous appearance is rapidly transformed to minute submembranous septin assemblies upon nocodazole treatment (Figure 9C, bottom; see enlarged view), that is, the same general appearance as in Vector-Co cells lacking microtubules (Sellin *et al.*, 2011a). Thus, whereas adequate levels of the SEPT9(a) isoform confer microtubule association, this isoform does not detectably alter the membrane-proximal arrangement of septin heteromers observed in cells with disrupted microtubules.

The arrangement of septins in cells in which octamers have either isoform SEPT9(e) or SEPT9(f) at their ends is shown in Figure 9D. It is evident that these octamers assemble into septin disks that are larger than observed in Vector-Co cells, which results in a more pronounced central clearing (compare enlarged images in Figure 9, A and D). Estimation of the average diameter shows that SEPT9(e) enlarges the septin disks even more than the SEPT9(f) isoform

(A) Images of representative control or SEPT9-depleted (shRNA[SEPT9]) cells in which heteromers are visualized by low-level coexpression of the SEPT7-AcGFP reporter. Deconvoluted optical sections at either the equatorial plane or parallel to the plasma membrane, as indicated at the top, are shown. Scale bar, 5 μm. (B) The size distribution of SEPT7-AcGFP visualized disk-like structures in vector control (N = 391; 31 cells analyzed) and SEPT9-depleted cells (N = 578; 30 cells analyzed) shown in A. Optical sections parallel to the plasma membrane were used for measurement. (C) Same as A, but the images show cells in which the endogenous SEPT9 isoforms were replaced with SEPT9(a). The effect of a brief nocodazole treatment is also shown (+Noc). (D) Same as A, but the images show cells in which the endogenous SEPT9 isoforms were replaced with either SEPT9(e) (top) or SEPT9(f) (bottom). (E) The appearance of SEPT7-AcGFP– visualized septin assemblies in the absence or presence of nocodazole (+Noc, 60–90 min) was evaluated by observation of live cells (N = 400 cells) as outlined in *Materials and Methods*. Individual interphase cells were evaluated on the criteria of cortical septin disk-like assemblies (open bars), elongated microtubule-like septin filaments (striped bars), and minute submembranous septin assemblies (shaded bars). The large majority of cells could be unambiguously classified into one of these three categories, and we did not note cells in which septin disk-like assemblies and microtubule-like septin filaments coexist. However, after nocodazole treatment we noted some cells in which septin disk-like assemblies coexist with minute submembranous septin assemblies. To minimize ambiguity, these cells were classified as having septin disk-like assemblies. The results in A–E are representative for at least two independently transfected cell lines of each SEPT9 isoform.
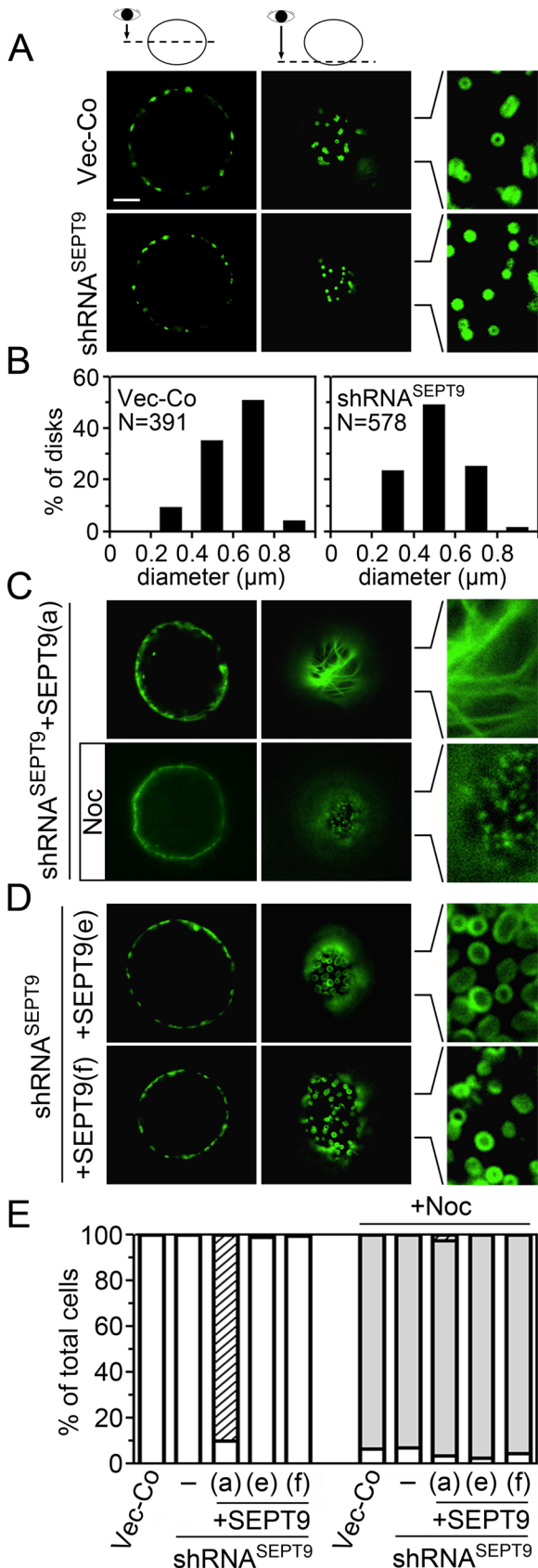
FIGURE 9: The localization of the SEPT7-AcGFP reporter in live cells that contain a predominant fraction of octameric heteromers with distinct SEPT9 isoforms at their tips. The cell lines characterized in Figure 8 were analyzed by epifluorescence microscopy of live cells.

(SEPT9(e), diameter 1.18 ± 0.28 μm; SEPT9(f), diameter 0.85 ± 0.17 μm; Vector-Co, diameter 0.59 ± 0.13 μm). These results confirm that octamers containing these short SEPT9 isoforms at their ends are incorporated into septin disks and modulate their size.

Figure 9E shows the frequencies of cells with various types of septin arrangements, which were scored according to previously defined criteria (Sellin et al., 2011a). The data demonstrate that the SEPT9(a) isoform confers microtubule association in the great majority of cells (striped bars). Moreover, after microtubule depolymerization by nocodazole, we found that each of the observed SEPT9 isoform–specific septin arrangements was altered to minute cortical assemblies (shaded bars). The appearances of these microtubule-independent assemblies seem unaffected by the depletion of endogenous SEPT9 isoforms or their replacement with any of the single isoforms (unpublished data). Thus all of the SEPT9 isoform-specific septin arrangements described in Figure 9 depend on an intact interphase microtubule array.

DISCUSSION

SEPT9 is the septin paralogue that is most convincingly linked to human disorders, and both its expression levels and isoform composition differ among cell types (for references, see Stanbery and Petty, 2012). The present cell model system consists of human cells of hematopoietic origin (K562), which express significant levels of SEPT2, SEPT5, SEPT6, SEPT7, SEPT8, and SEPT11, as well as three of the six confirmed SEPT9 isoforms (Figures 1 and 3; Sellin et al., 2011b). The native septin heteromer pool of these cells comprises a mixture of hexamers and octamers in which the subunits appear arranged according to their membership in any of the four homology-based subgroups (see Figure 4; Sellin et al., 2011b). Although, predictably, all hexamers are capped by SEPT7, octamers are heterogeneous with respect to the SEPT9 isoform at their ends. These previous findings provide a conceptual framework in which to consider the function of the 13 mammalian septin paralogues and their isoforms.

In this study we replaced endogenous SEPT9 gene products with individual native or AcGFP-tagged SEPT9 isoforms expressed at sufficient levels to generate a predominantly octameric heteromer pool among the majority of cells (Figure 4 and Supplemental Figure S1). These genetically manipulated cell lines allowed us to address the significance of changes of the octamer-to-hexamer ratio, as well as functional properties of individual SEPT9 isoforms. Taken together, our results support the following conclusions: 1) cell type–specific SEPT9 isoform composition and the octamer-to-hexamer ratio are major determinants of higher-order arrangements of the septin system; 2) hexamers and octamers may polymerize into common microtubule-supported structures such as submembranous septin disks in nonadhered cells; 3) both hexamers and octamers associate with artificially bundled microtubules; and 4) SEPT9-conferred association to native microtubules is stabilized by cooperative heteromer interactions that require the N-terminal extension of the SEPT9(a) isoform. The evidence supporting these conclusions is discussed in what follows.

The significance of cell type–specific SEPT9 isoform composition and the octamer-to-hexamer ratio for higher-order septin arrangements

Our evidence support that the AcGFP-SEPT9(a) isoform reporter visualizes authentic assemblies of SEPT9(a)-containing octamers (Figures 5 and 9). The reporter visualized two distinct arrangements; however, we did not observe both of these within the same cell. An essential premise for interpreting these findings is that the

fluorescence intensity correlates with the octamer-to-hexamer ratio of individual cells (Supplemental Figures S1 and S2 support this prediction). Thus, scoring of live cells in which endogenous SEPT9 was replaced by AcGFP-tagged SEPT9 isoforms provides information on how higher-order septin arrangements are altered by changes in the octamer-to-hexamer ratio of septin heteromers. Inspection of the minority of cells in which the octamer-to-hexamer ratio is predictably low (i.e., weak AcGFP fluorescence) shows that SEPT9(a)-containing octamers are solely assembled into submembranous punctuate structures, which are distinct from elongated, microtubule-like structures. Given a predominant octameric pool in the major cell population (Supplemental Figure S1), it can be concluded that SEPT9(a)-mediated microtubule-association—and the absence of submembranous punctuate structures—seen in most cells is coupled to a high octamer-to-hexamer ratio.

The outlined data, combined with cognate analysis based on detection by means of a SEPT7-AcGFP reporter, suggest a propensity of octamers (as visualized by the AcGFP-SEPT9(a) isoform) to localize to the same locations as the total septin pool (as visualized by SEPT7-AcGFP). This is consistent with the finding that the SEPT9(a) expression level in wild-type K562 cells (Figures 1 and 4) is insufficient to confer detectable microtubule association (Figure 9A). These observations suggest that the total septin pool (octamers and hexamers) function together as a single septin system.

The present studies of wild-type K562 cells support the notion that mammalian interphase cells in general only contain a single type of septin arrangement. Thus analysis of microtubule-dependent cell retention of septins revealed no differences between octamers and hexamers or among SEPT9 isoforms (Figure 6A). Moreover, in cells expressing the SEPT9(a) isoform, all endogenous septins analyzed appear equally represented in heteromers retained by nonbundled microtubules (Figure 7E). We also noted indistinguishable partitioning of individual septins during cell permeabilization at low ionic strengths (Figure 2), which was also observed in epithelial (HeLa) and lymphoid (Jurkat) cell lines (unpublished observations). Thus it seems that the extraordinary heterogeneous septin heteromer pool of mammalian cells has a propensity to combine into joint higher-order arrangements. However, this propensity is less apparent during cell division, which is due to disassembly of interphase-specific septin structures at the entry of mitosis, followed by a gradual accumulation at the contractile ring (Sellin et al., 2011a).

Higher-order septin arrangements observed in nonadherent cell types depend on the interphase microtubule array

Septin disks are the sole discernible interphase septin arrangement in nonadhered myeloid and lymphoid cells such as K562 and Jurkat cells. These structures occupy ~8% of the inner leaflet of the plasma membrane of nonadhered cells but transform into other arrangements in response to microtubule-directed drugs or cell adherence to integrin-activating ligands (Sellin et al., 2011a). The present study shows that SEPT9 is not required for the septin disk arrangement per se, but the octamer-to-hexamer ratio and SEPT9 isoform composition are clearly of significance for its size (Figure 9).

Disruption of actin bundles in epithelial and fibroblast cell lines by actin-targeting drugs causes the emergence of ring-like septin structures in the cytosol, which are generated by rolling up of linear septin filaments that dissociate from actin bundles (Kinoshita et al., 2002). Of interest, SEPT9 depletion has been shown to decrease the size range of the free-floating septin rings that develop upon treatment of HeLa cells with the actin drug cytochalasin D (Kim et al., 2011). Although these data suggest a similar septin arrangement in

free-floating rings and septin disks, the latter are distinguished by an exclusive submembranous localization and a dependence on microtubules for structural integrity.

We previously showed that a brief expose to Taxol (3 min, 3 µM) preserves septin disks in permeabilized cells (Sellin et al., 2011a). The present analysis links this observation to Taxol-promoted microtubule bundling (Figure 6A). Hence the septin disk arrangement seems likely to be supported by dynamic interactions with the dense array of cortical microtubules that are typical for nonadhered spherical cells. This contrasts with the stable microtubule association conferred by the SEPT9(a) isoform (Figures 8B and 9C). It is notable that the SEPT9(a)-AcGFP reporter, which has an unperturbed N-terminal extension and exists in cells as monomers, appears entirely nonlocalized (Sellin et al., 2011a). This is as predicted by a mechanism involving cooperative heteromer interactions along microtubules. Thus there is no evidence that the N-terminal extension of SEPT9(a) has an autonomous ability to associate with microtubules.

Septin interactions with microtubules in mammalian cells have been a long-standing issue. Even so, we are not aware of any confirmed evidence indicating a direct binding of septins to microtubules. Moreover, the N-terminal extension of the SEPT9(a) isoform does not have any recognizable microtubule-interaction domain. Thus it seems more likely that the interactions occur indirectly through some adaptor. Such a scenario would be analogous to septin association to actin bundles, which depends on adaptor proteins such as anillin (Kinoshita et al., 2002).

Functional consequences of AcGFP fusion to the variable N-terminal extension of SEPT9 isoforms

AcGFP fusion to the SEPT9 C-terminus has been found to effectively block assembly into heteromers (Sellin et al., 2011a). It follows that specific visualization of octamers requires AcGFP fusion to the N-terminal end of SEPT9 reporters. However, this study shows that fusion to the variable N-terminus may affect assembly into higher-order structures and that SEPT9 isoforms are differentially affected. A case in point is that septin disk enlargement by SEPT9 isoforms lacking the N-terminal extension of SEPT9(a) is not seen using the cognate AcGFP-tagged isoforms, which were nonlocalized in most cells (compare Figures 5 and 9D).

Deletion of the α0 helix at the N-terminal end of the budding yeast septin CDC11 weakens homotypic CDC11–CDC11 interactions at the NC-interface of octamers, which prevents end-to-end heteromer polymerization (Bertin et al., 2008; McMurray et al., 2011). Moreover, expression of SEPT9 lacking the entire N-terminus, including the α0 helix, has been shown to disrupt septin filament formation, which supports the notion that octamers polymerize through a SEPT9–SEPT9 NC-interface (Kim et al., 2011). It is notable that AcGFP fusion at the short N-terminal extension of the SEPT9(e) and SEPT9(f) isoforms also results in octamers that appear defective in their polymerization. Thus, in analogy with the effect of removing the α0 helix of SEPT9, AcGFP fusion proximal to the N-terminal end of the SEPT9 G-domain may obstruct SEPT9–SEPT9 NC-interface docking, which would predictably interfere with octamer end-to-end polymerization.

The SEPT9(a) isoform has a 295-residue N-terminal extension, whereas the N-terminus of SEPT9(f) extends only 44 residues from the G-domain. All our evidence supports that the AcGFP-SEPT9(a) isoform reporter visualizes authentic octamer localizations in live cells with intact microtubules. However, the AcGFP-SEPT9(a) isoform reporter appears nonlocalized in nocodazole-treated cells, irrespective of their fluorescence levels, whereas the SEPT7-AcGFP reporter visualizes cortical assemblies under the cognate

experimental conditions (compare Figures 5E and 9C; also, unpublished data). Moreover, the septin disks visualized by this reporter appear somewhat distorted (Figure 5C). These effects by AcGFP fusion may reflect a partial interference at the SEPT9–SEPT9 NC-interface, which would support the notion that stable SEPT9(a)-conferred association involves heteromer polymerization along microtubules.

Concluding remarks

The native septin hetero-oligomer pool of budding yeast and other fungi has to our knowledge not been analyzed with sufficient resolution to address the question of whether the number of septin subunits of core hetero-oligomers may vary. Even so, a recent report indicates that alternative terminal subunits of octameric septin heteromers are a feature that is conserved across kingdoms. Thus, in budding yeast, both Cdc11 and Shs1 may form a stable G-interface with Cdc12 and thereby serve as alternative terminal subunits of octameric hetero-oligomers (Garcia et al., 2011). In apparent analogy with our studies of SEPT9 isoforms in intact human cells, Cdc11 and Shs1 were shown to confer differential higher-order filamentous arrangements to bacterially expressed octameric hetero-oligomers when diluted in a low-salt buffer. In addition, the ratio of Cdc11- and Shs1-containing hetero-oligomers was shown to direct both the overall arrangement and the size of the circular structures formed by Shs1-containing octamers (Garcia et al., 2011).

Septins have been reported to localize to spindle microtubules in epithelial cell types (Spiliotis et al., 2005), as well as a microtubule-containing bridge, termed the midbody, and the contractile ring during late telophase (Estey et al., 2010). Microtubule-proximal localization is not detected during mitosis of myeloid and lymphoid cells such as K562 and Jurkat cells (Sellin et al., 2011a). Nevertheless, adequate levels of SEPT9(a) result in localization of the SEPT7-AcGFP reporter to the mitotic spindle, and, during late mitosis, we noted simultaneous localization to microtubules at the midbody and the contractile ring (unpublished data). Of interest, SEPT9-depletion of HeLa cells results in late abscission defects during cytokinesis, which are reportedly rescued by SEPT9(a) but not the SEPT9(c) or SEPT9(d) isoforms (Estey et al., 2010). Thus our results are consistent with a reported SEPT9(a) isoform–specific function in HeLa cells, and the combined evidences suggest that this isoform is required to confer microtubule association of septins during mitotic exit of epithelial cell types.

MATERIALS AND METHODS
Shuttle vector DNA constructs

The Epstein-Barr virus (EBV)-based shuttle vector directing constitutive expression of short hairpin RNA (shRNA) targeting mRNAs encoding SEPT7, termed shRNA[SEPT7], has been described (Sellin et al., 2011b). The cognate SEPT9 mRNA targeting derivative, termed shRNA[SEPT9], was constructed by an analogous strategy (the targeted sequence is located within the G-domain, accession NM_001113491.1; CAC CAC ACA CTG TGA GTT T). The EBV-based pMEP4 shuttle vectors directing regulatable expression of SEPT7-AcGFP and SEPT9(a)-AcGFP, which contain the AcGFP fluorescent reporter at their C-terminal ends, have been described (Sellin et al., 2011a,b). Construction of pMEP vectors directing regulatable expression of native and AcGFP-fused SEPT9 isoforms, which were all immune to shRNA[SEPT9]-mediated suppression due to four silent mutations within the 19-nucleotide targeting sequence, are detailed in the Supplemental Materials and Methods. The coding sequences of PCR-generated fragments were confirmed by nucleotide sequence analysis.

Cell culture, gene product replacement, and generation of transfected cell lines

The human myeloid K562 cell line was cultured in RPMI 1640 supplemented with insulin (5 mg/l), transferrin (5 mg/l), sodium selenite (5 μg/l), and 5% fetal calf serum. The general procedure for transfection with shuttle vectors and selection of hygromycin-resistant cell lines has been described (Holmfeldt et al., 2007). Constitutive expression from the hMTIIa promoter was obtained by cultivation of cells in standard RPMI medium. The general protocols used for gene product replacement have been described (Holmfeldt et al., 2007). For replacement of endogenous SEPT9 isoforms with single native or AcGFP-tagged SEPT9 isoforms, K562 cells were transfected with a mixture of 2 μg of shRNA[SEPT9], 4 μg of the indicated shRNA[SEPT9]-resistent pMEP-SEPT9 isoform derivative, and empty pMEP4 vector up to a total of 16 μg of DNA. For depletion of SEPT7 or SEPT9, K562 cells were transfected with a mixture of 2 μg of shRNA[SEPT7] or shRNA[SEPT9], as indicated in the text, and empty pMEP4 vector up to a total of 16 μg of DNA. Owing to the stringent replication control of the EBV-based vector, the ratio of transfected DNAs is stable for several weeks (Melander Gradin et al., 1997).

Analysis of microtubule content, proteins, and mRNA

The total content of microtubules in cells was determined by flow cytometry as detailed in Sellin et al. (2008). To estimate the total amount of polymerizable tubulin, cells were treated with the polymerization-promoting drug Taxol (15 min, 2 μM), which allowed calculation of tubulin heterodimer–polymer partitioning. Immunoblotting was performed using the α-tubulin, HSP70, green fluorescence protein, Oncoprotein 18/Stathmin (Op18), vimentin, and septin antibodies described in Sellin et al. (2011a). For quantification of mRNA, quantitative RT-PCR (qRT-PCR) was used as described (Sellin et al., 2008). PCRs were performed in triplicate using primer pairs specific for SEPT9 transcript variants 1–7, which were designed using the Primer-Blast software developed at the National Center for Biotechnology Information (www.ncbi.nlm.nih.gov/genome). Primer pairs and PCR product lengths are listed in the Supplemental Materials and Methods.

Fluorescence microscopy, density-gradient centrifugation, and determination of protein partitioning between soluble and insoluble states

Live and fixed cells were examined by fluorescence microscopy as detailed in Sellin et al. (2011a). Septin assemblies were scored by observation of live SEPT7-AcGFP–expressing cells according to previously described criteria (Sellin et al., 2011a). Cells containing aggregates of the SEPT7-AcGFP reporter (2–5%) were excluded from the analysis. The heteromeric context of septins was evaluated by density-gradient centrifugation as described in Brannstrom et al. (2009) and Sellin et al. (2011b). In brief, cells were gently resuspended on ice in the presence of 0.2% saponin and 10 μg/ml leupeptin in 80 mM PIPES (pH 6.9), 2 mM $MgCl_2$, 4 mM ethylene glycol, and tetraacetic acid (PEM buffer). The particulate cell fraction was removed by centrifugation (10 min, 14,000 × g). The current protocol results in recovery of >95% of all septins in the supernatant (Sellin et al., 2011b). To ensure complete disassembly of septin filaments, the supernatant was supplemented with 0.5 M NaCl prior to density-gradient centrifugation. Protein partitioning between soluble and insoluble states was analyzed by two distinct protocols, both of which involved permeabilization of cells by a saponin-containing buffer. The first protocol involved Western blot detection of proteins retained and released subsequent to cell permeabilization as previously described (3 min at 37°C in PEM buffer with 0.2%

saponin; Sellin et al., 2011a). For quantitative analysis of Western blots, the Bio-Rad ChemiDoc (Bio-Rad, Hercules, CA) system was used with the Quantity One 4.4 program. The second protocol is based on detection of AcGFP-tagged septins before and after cell permeabilization. Cells were gently resuspended at 37°C in standard RPMI growth media supplemented with 5 mM ethylene glycol tetraacetic acid, followed by addition of an equal volume of a permeabilization buffer (PEM buffer with 0.2% saponin). After 20 min at 37°C, the AcGFP-fluorescence intensity of individual cells was analyzed by flow cytometry. Calculations of the percentage of AcGFP-tagged septins retained by permeabilized cells were based on the mean fluorescence intensity of the cell population before and after cell permeabilization. Note that standard RPMI growth media has twice the ionic strength of PEM buffer, which in combination with 20-min incubation of permeabilized cells at 37°C results in increased stringency compared with the first protocol, in which cells were only incubated for 3 min in PEM buffer with 0.2% saponin. This increase in stringency facilitated detection of an increased stability of septin heteromer retention by permeabilized cells.

Analysis of septin heteromers by Blue native PAGE

Septins were recovered by permeabilizing cells (60 × 10⁶ cells/ml, 10 min on ice) in a saponin-containing PEM buffer, which was supplemented with 25 mM ε-aminocapric acid, 10 μg/ml leupeptin, and 10 μg/ml Pefabloc. The released soluble proteins were recovered by centrifugation (10 min, 14,000 × g) and supplemented with NaCl to a final concentration of 0.45 M. After 15 min on ice, the sample was clarified by centrifugation (10 min, 14,000 × g) and then passed over a desalting column (30-kDa cut off, Micro Bio-Spin P30 Column; Bio-Rad) that was equilibrated in a buffer containing 10 mM phosphate, pH 7.5, 0.45 M NaCl, 25 mM ε-aminocapric acid, and 1 mM ethylene glycol tetraacetic acid. The recovered proteins were mixed with glycerol (50% final concentration) and stored at −20°C until analysis. As evidenced by Western blotting, essentially all septins were recovered by the present protocol. For analysis by Blue native PAGE, we used the Novex NativePAGE Bis-Tris Gel System precast polyacrylamide gel system (Invitrogen, Carlsbad, CA). Electrophoresis (4–16% NativePAGE gels) and immunodetection of protein complexes were performed according to the supplier recommendations.

REFERENCES

Beise N, Trimble W (2011). Septins at a glance. J Cell Sci 124, 4141–4146.

Bertin A, McMurray MA, Grob P, Park SS, Garcia G 3rd, Patanwala I, Ng HL, Alber T, Thorner J, Nogales E (2008). Saccharomyces cerevisiae septins: supramolecular organization of heterooligomers and the mechanism of filament assembly. Proc Natl Acad Sci USA 105, 8274–8279.

Bertin A, McMurray MA, Thai L, Garcia G 3rd, Votin V, Grob P, Allyn T, Thorner J, Nogales E (2010). Phosphatidylinositol-4,5-bisphosphate promotes budding yeast septin filament assembly and organization. J Mol Biol 404, 711–731.

Bowen JR, Hwang D, Bai X, Roy D, Spiliotis ET (2011). Septin GTPases spatially guide microtubule organization and plus end dynamics in polarizing epithelia. J Cell Biol 194, 187–197.

Brannstrom K, Sellin ME, Holmfeldt P, Brattsand M, Gullberg M (2009). The Schistosoma mansoni protein Sm16/SmSLP/SmSPO-1 assembles into a nine-subunit oligomer with potential to inhibit Toll-like receptor signaling. Infect Immun 77, 1144–1154.

Cao L, Ding X, Yu W, Yang X, Shen S, Yu L (2007). Phylogenetic and evolutionary analysis of the septin protein family in metazoan. FEBS Lett 581, 5526–5532.

Estey MP, Di Ciano-Oliveira C, Froese CD, Bejide MT, Trimble WS (2010). Distinct roles of septins in cytokinesis: SEPT9 mediates midbody abscission. J Cell Biol 191, 741–749.

Field CM, al-Awar O, Rosenblatt J, Wong ML, Alberts B, Mitchison TJ (1996). A purified *Drosophila* septin complex forms filaments and exhibits GTPase activity. J Cell Biol 133, 605–616.

Fuchtbauer A, Lassen LB, Jensen AB, Howard J, Quiroga Ade S, Warming S, Sorensen AB, Pedersen FS, Fuchtbauer EM (2011). Septin9 is involved in septin filament formation and cellular stability. Biol Chem 392, 769–777.

Garcia G 3rd, Bertin A, Li Z, Song Y, McMurray MA, Thorner J, Nogales E (2011). Subunit-dependent modulation of septin assembly: budding yeast septin Shs1 promotes ring and gauze formation. J Cell Biol 195, 993–1004.

Garrenton LS, Stefan CJ, McMurray MA, Emr SD, Thorner J (2010). Pheromone-induced anisotropy in yeast plasma membrane phosphatidylinositol-4,5-bisphosphate distribution is required for MAPK signaling. Proc Natl Acad Sci USA 107, 11805–11810.

Hanai N, Nagata K, Kawajiri A, Shiromizu T, Saitoh N, Hasegawa Y, Murakami S, Inagaki M (2004). Biochemical and cell biological characterization of a mammalian septin, Sept11. FEBS Lett 568, 83–88.

Holmfeldt P, Stenmark S, Gullberg M (2007). Interphase-specific phosphorylation-mediated regulation of tubulin dimer partitioning in human cells. Mol Biol Cell 18, 1909–1917.

John CM *et al.* (2007). The *Caenorhabditis elegans* septin complex is nonpolar. EMBO J 26, 3296–3307.

Kim MS, Froese CD, Estey MP, Trimble WS (2011). SEPT9 occupies the terminal positions in septin octamers and mediates polymerization-dependent functions in abscission. J Cell Biol 195, 815–826.

Kinoshita M (2003). Assembly of mammalian septins. J Biochem 134, 491–496.

Kinoshita M, Field CM, Coughlin ML, Straight AF, Mitchison TJ (2002). Self- and actin-templated assembly of mammalian septins. Dev Cell 3, 791–802.

Martinez C, Corral J, Dent JA, Sesma L, Vicente V, Ware J (2006). Platelet septin complexes form rings and associate with the microtubular network. J Thromb Haemost 4, 1388–1395.

McMurray MA, Thorner J (2008). Septin stability and recycling during dynamic structural transitions in cell division and development. Curr Biol 18, 1203–1208.

McMurray MA, Thorner J (2009). Septins: molecular partitioning and the generation of cellular asymmetry. Cell Div 4, 18.

McMurray MA, Bertin A, Garcia G 3rd, Lam L, Nogales E, Thorner J (2011). Septin filament formation is essential in budding yeast. Dev Cell 20, 540–549.

Melander Gradin H, Marklund U, Larsson N, Chatila TA, Gullberg M (1997). Regulation of microtubule dynamics by Ca2+/calmodulin-dependent kinase IV/Gr-dependent phosphorylation of oncoprotein 18. Mol Cell Biol 17, 3459–3467.

Mostowy S, Cossart P (2012). Septins: the fourth component of the cytoskeleton. Nat Rev Mol Cell Biol 13, 183–194.

Nagata K *et al.* (2003). Filament formation of MSF-A, a mammalian septin, in human mammary epithelial cells depends on interactions with microtubules. J Biol Chem 278, 18538–18543.

Oh Y, Bi E (2011). Septin structure and function in yeast and beyond. Trends Cell Biol 21, 141–148.

Pan F, Malmberg RL, Momany M (2007). Analysis of septins across kingdoms reveals orthology and new motifs. BMC Evol Biol 7, 103.

Sellin ME, Holmfeldt P, Stenmark S, Gullberg M (2008). Global regulation of the interphase microtubule system by abundantly expressed Op18/Stathmin. Mol Biol Cell 19, 2897–2906.

Sellin ME, Holmfeldt P, Stenmark S, Gullberg M (2011a). Microtubules support a disk-like septin arrangement at the plasma membrane of mammalian cells. Mol Biol Cell 22, 4588–4601.

Sellin ME, Sandblad L, Stenmark S, Gullberg M (2011b). Deciphering the rules governing assembly order of mammalian septin complexes. Mol Biol Cell 22, 3152–3164.

Sheffield PJ, Oliver CJ, Kremer BE, Sheng S, Shao Z, Macara IG (2003). Borg/septin interactions and the assembly of mammalian septin heterodimers, trimers, and filaments. J Biol Chem 278, 3483–3488.

Sirajuddin M, Farkasovsky M, Hauer F, Kuhlmann D, Macara IG, Weyand M, Stark H, Wittinghofer A (2007). Structural insight into filament formation by mammalian septins. Nature 449, 311–315.

Sirajuddin M, Farkasovsky M, Zent E, Wittinghofer A (2009). GTP-induced conformational changes in septins and implications for function. Proc Natl Acad Sci USA 106, 16592–16597.

Spiliotis ET, Gladfelter AS (2011). Spatial guidance of cell asymmetry: septin GTPases show the way. Traffic 13, 195–203.

Spiliotis ET, Kinoshita M, Nelson WJ (2005). A mitotic septin scaffold required for Mammalian chromosome congression and segregation. Science 307, 1781–1785.

Stanbery L, Petty EM (2012). Steps solidifying a role for SEPT9 in breast cancer suggest that greater strides are needed. Breast Cancer Res 14, 101.

Surka MC, Tsang CW, Trimble WS (2002). The mammalian septin MSF localizes with microtubules and is required for completion of cytokinesis. Mol Biol Cell 13, 3532–3545.

Tanaka-Takiguchi Y, Kinoshita M, Takiguchi K (2009). Septin-mediated uniform bracing of phospholipid membranes. Curr Biol 19, 140–145.

Weirich CS, Erzberger JP, Barral Y (2008). The septin family of GTPases: architecture and dynamics. Nat Rev Mol Cell Biol 9, 478–489.

Wittig I, Braun HP, Schagger H (2006). Blue native PAGE. Nat Protoc 1, 418–428.